Pergamon

Int. J. Heat Mass Transfer. Vol. 40, No. 1, pp. 131–139, 1997
Copyright © 1996 Elsevier Science Ltd
Printed in Great Britain. All rights reserved
0017–9310/97 $15.00 + 0.00

PII: S0017–9310(96)00083–X

Multicomponent diffusion interactions during condensation in laminar and turbulent pipe flow

M. BRAUN and U. RENZ†

RWTH Aachen, Lehrstuhl für Wärmeübertragung and Klimatechnik, 52056 Aachen, Germany

(*Received* 31 *August* 1995 *and in final form* 29 *January* 1996)

Abstract—The coupled heat and mass transfer between two separated cocurrently flowing phases in vertical pipes is examined. A numerical approach based on the two-dimensional boundary layer equations is presented and validated with experiments available in literature. The effects of multicomponent diffusion interactions on the mass fraction profiles are demonstrated at the point of osmotic diffusion of one component during condensation of two components. The coupling of the concentration profiles increases with Reynolds number and leads to countercurrent gradients even at cocurrent concentration differences. The results agree well with available experimental data. Copyright © 1996 Elsevier Science Ltd.

1. INTRODUCTION

Industrial heat and mass exchange processes often involve multicomponent mixtures. These processes are not only influenced by the coupling of heat and mass transfer but also by multicomponent diffusion interactions leading to special mass transport phenomena, such as diffusion barrier, osmotic diffusion and reverse diffusion as pointed out by Toor [1]. The interaction effects can be described by the Stefan–Maxwell equations as well as by the generalized Fick's law.

Several matrix methods have been developed to extend the description of mass transfer to multicomponent mixtures. Toor [2] and Stewart and Prober [3] developed their linearized theories on the basis of the generalized Fick's law assuming negligible concentration changes along the diffusion path. The matrix method of Krishna and Standart [4] is based upon the Stefan–Maxwell equations. They solved the problem of concentration dependency by reducing the multicomponent diffusion problem to a system of coupled binary diffusion problems. To do so they used the assumption that the concentration layer thickness is the same for all binary diffusion problems. These methods are applied to flow problems by the penetration or film theories and require empirical correlations for the exchange coefficients.

Besides these one-dimensional approaches several solutions of the two-dimensional (2D) coupled heat and mass transfer problem in laminar flow exist. Taitel and Tamir [5] were the first to solve the 2D boundary layer equations for a condensing stagnant ternary system coupled with a condensate film flowing down a vertical plate. They assumed constant temperature and constant properties in the multicomponent gas mixture. Sage and Estrin [6] extended this approach by adding the solution of the energy equation and used it to investigate supersaturation and separation effects in free convective flow. Kosuge *et al.* [7] and Bröcker [8] solved the equation set of Taitel and Tamir for laminar flow over a flat plate without considering heat transfer. Later Bröcker [9] extended his approach to coupled heat and mass transfer problems but did not include the coupling with a liquid film.

All these approaches deal with stagnant surroundings or laminar flows. For turbulent flow some extensions of the matrix methods exist using a given eddy kinematic viscosity profile [10, 11]. But for this extension the multicomponent diffusion coefficients have to be constant along the diffusion path. Two-dimensional solutions of the turbulent boundary layer equations have been performed for partial condensation of one vapour component on flat surfaces by Renz [12] and within pipes by Odenthal [13] and for evaporation of a binary liquid film in vertical pipes by Baumann and Thiele [14]. The latter neglect multicomponent diffusion interactions by using effective diffusion coefficients for mass transport.

In the following sections results of numerical investigation are presented looking mainly at the influence of multicomponent diffusion interactions on mass transfer in partial binary condensation in turbulent pipe flow [15]. A numerical procedure to solve the coupled system of conservation equations for both the vapour–gas and the liquid phase has been established and validated with experiments available in literature. The effects of multicomponent diffusion interactions on the turbulent concentration profiles will be examined at the point of osmotic diffusion.

† Author to whom correspondence should be addressed.

NOMENCLATURE

$c_1, c_2, c_3, c_4, c_\eta$ constants for the k, ε-model
c_p specific heat capacity
d pipe diameter
D_{ij} multicomponent diffusion coefficient
$\mathscr{D}_{ij}$ binary diffusion coefficient of species 'i' in inert gas 'j'
f_1, f_2, f_η functions for the k, ε-model
g gravity constant
h specific enthalpy
$\hat{h} = h + u^2/2$ total specific enthalpy
Δh_V heat of vaporization
$\vec{j}''$ diffusion flux density
k turbulent kinetic energy
$\dot{m}$ mass flow rate
$\dot{m}''$ mass flux density
p pressure
Pr Prandtl number
$\dot{q}''$ heat flux density
r radial coordinate
R pipe radius
Re Reynolds number
Sc Schmidt number
T temperature
u axial velocity
u_τ friction velocity
v radial velocity
x diffusion layer coordinate
y wall distance
z axial coordinate.

Greek symbols
ε turbulent energy dissipation
δ diffusion layer thickness
η dynamic viscosity
λ thermal conductivity
ρ density
$\sigma_k, \sigma_\varepsilon$ constants of the k, ε-model
τ shear stress
ν kinematic viscosity
ϑ temperature
ϑ_τ due point temperature
ξ mass fraction
Ψ mole fraction.

Subscripts
A side A of diffusion layer
B side B of diffusion layer
c centre
E entrance
F film
I gas–liquid interface
i, j species i, j
O outlet
t turbulent
1, 2, 3 species 1, 2, 3
W wall.

2. MODEL AND EQUATIONS

In this work the partial filmwise condensation of two vapours forming a mixture with a non-condensable gas is considered inside a vertical tube with cocurrent downward flow of both the gaseous and the liquid phase. Momentum, heat and mass transfer between both phases lead to developing profiles of velocity u, temperature T and mass fractions ξ_i, see Fig. 1. These profiles can be described by two sets of conservation equations for the gaseous and the liquid phase which are coupled by boundary conditions at the interface. Secondary effects such as thermal diffusion, radiation and surface tension are neglected.

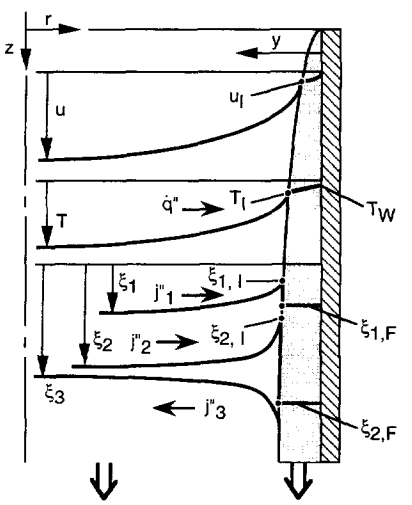

Fig. 1. Ternary two phase flow in vertical pipe flow.

2.1. *Vapour–gas flow*

The turbulent flow of a vapour–gas mixture with n components in axisymmetric geometry is described by the following set of differential equations (mixture properties have no subscript):

continuity equation

$$\frac{\partial(\rho u)}{\partial z} + \frac{1}{r}\frac{\partial(\rho r v)}{\partial r} = 0 \qquad (1)$$

z-momentum equation

$$\rho u\frac{\partial u}{\partial z} + \rho v\frac{\partial u}{\partial r} = -\frac{1}{r}\frac{\partial(r\tau)}{\partial r} + \rho g - \frac{\mathrm{d}p}{\mathrm{d}z} \qquad (2)$$

energy equation

$$\rho u\frac{\partial \hat{h}}{\partial z}+\rho v\frac{\partial \hat{h}}{\partial r}=-\frac{1}{r}\frac{\partial(r\dot{q}''+ru\tau)}{\partial r}+\rho ug \tag{3}$$

species conservation equation

$$\rho u\frac{\partial \xi_i}{\partial z}+\rho v\frac{\partial \xi_i}{\partial r}=-\frac{1}{r}\frac{\partial(r\dot{j}_i'')}{\partial r}. \tag{4}$$

The formulation for the flux terms are given as follows:

shear stress

$$\tau=\underbrace{-\eta\frac{\partial u}{\partial r}}_{\text{laminar shear}}\underbrace{-\eta_t\frac{\partial u}{\partial r}}_{\text{laminar shear}} \tag{5}$$

heat flux

$$\dot{q}''=\underbrace{-\frac{\eta}{Pr}c_p\frac{\partial T}{\partial r}}_{\text{conduction}}+\underbrace{\sum_{i=1}^{n}h_i\dot{j}_i''}_{\text{diffusion}}\underbrace{-\frac{\eta_t}{Pr_t}c_p\frac{\partial T}{\partial r}}_{\text{turbulent heat transport}} \tag{6}$$

mass flux

$$\dot{j}_i''=\underbrace{\underbrace{-\rho D_{ii}\frac{\partial \xi_i}{\partial r}}_{\text{diagonal term}}\underbrace{-\rho\sum_{\substack{j=1\\ j\neq i}}^{n-1}D_{ij}\frac{\partial \xi_j}{\partial r}}_{\text{cross terms}}}_{\text{molecular diffusion}}\underbrace{-\frac{\eta_t}{Sc_t}\frac{\partial \xi_i}{\partial r}}_{\text{turbulent diffusion}}. \tag{7}$$

Due to the prediction of a flow problem, diffusion is described in the mass reference frame. The mass flux terms are calculated by the generalized Fick's law where the diagonal term describes the molecular diffusion due to the concentration gradient of the considered species. The coupling with the other species in multicomponent mixtures is included in the cross terms. Equations for the multicomponent diffusion coefficients can be derived from Stefan–Maxwell equations and are given in [4, 6].

The turbulent Prandtl and Schmidt numbers were taken to be 0.9. This is a good assumption for gaseous systems with molecular Prandtl and Schmidt numbers greater that 0.3. The turbulent viscosity η_t is obtained from the k,ε-turbulence model of Jones and Launder [16].

turbulent kinetic energy k

$$\rho u\frac{\partial k}{\partial z}+\rho v\frac{\partial k}{\partial r}=\frac{1}{r}\frac{\partial}{\partial r}\left(\left(\eta+\frac{\eta_t}{\sigma_k}\right)r\frac{\partial k}{\partial r}\right)+\eta_t\left(\frac{\partial u}{\partial r}\right)^2-\rho\varepsilon-c_4\eta\left(\frac{\partial\sqrt{k}}{\partial r}\right)^2 \tag{8}$$

turbulent energy dissipation ε

$$\rho u\frac{\partial \varepsilon}{\partial z}+\rho v\frac{\partial \varepsilon}{\partial r}=\frac{1}{r}\frac{\partial}{\partial r}\left(\left(\eta+\frac{\eta_t}{\sigma_\varepsilon}\right)r\frac{\partial \varepsilon}{\partial r}\right)+c_3\frac{\eta\eta_t}{\rho}\left(\frac{\partial^2 u}{\partial r^2}\right)^2+c_1f_1\frac{\varepsilon}{k}\eta_t\left(\frac{\partial u}{\partial r}\right)^2-c_2f_2\frac{\rho\varepsilon^2}{k}. \tag{9}$$

The turbulent viscosity η_t can be estimated by

$$\eta_t=c_\eta f_\eta\frac{\rho k^2}{\varepsilon}. \tag{10}$$

The coefficient set of Kawamura [17] is used.

2.2. *Liquid flow*

The condensate film is considered to be laminar. Using the assumptions of the Nusselt theory the following set of conservation equations can be derived:

continuity equation

$$\frac{\partial(\rho_F u_F)}{\partial z}+\frac{1}{r}\frac{\partial(r\rho_F v_F)}{\partial r}=0 \tag{11}$$

z-momentum equation

$$0=\frac{1}{r}\frac{\partial\left(r\eta_F\dfrac{\partial u_F}{\partial r}\right)}{\partial r}+\rho_F g-\frac{\mathrm{d}p}{\mathrm{d}z} \tag{12}$$

energy equation

$$0=\frac{1}{r}\frac{\partial\left(r\lambda_F\dfrac{\partial T_F}{\partial r}\right)}{\partial r}. \tag{13}$$

A species conservation equation cannot be solved without considering the convective terms, because a zero mass fraction gradient is given as boundary condition at the wall. For simplicity a well mixed liquid film is assumed. The liquid mass fraction is given by

$$\xi_{F,i}=\frac{\dot{m}_{F,i}}{\sum_j\dot{m}_{F,j}}. \tag{14}$$

2.3. *Boundary and interface conditions*

The vapour–gas and the liquid flow are subject to the following boundary conditions: at the wall the no-slip condition is valid and a constant wall temperature is given. On the tube axis the gradients of u, $\hat{h}$, ξ_i, k and ε will be zero due to pipe symmetry. The two sets of non-linear partial differential equations for the vapour–gas and liquid flow, equations (1)–(4) and (11)–(14), are coupled at the liquid interface due to the equality of velocity, temperature and the vapour–liquid equilibrium. These unknown values can be calculated by local differential balances of momentum flux, heat flux and the species and mass fluxes

$$\eta_F\frac{\partial u_F}{\partial r}\bigg|_I=\eta\frac{\partial u}{\partial r}\bigg|_I \tag{15}$$

$$\lambda_F\frac{\partial T_F}{\partial r}\bigg|_I=\lambda\frac{\partial T}{\partial r}\bigg|_I+\sum_{j=1}^{n}\dot{m}_j''\Delta h_v|_I \tag{16}$$

$$\dot{m}_i''|_I = \dot{j}_i''|_I + \xi_i|_I \sum_{j=1}^{n} \dot{m}_j''|_I. \quad (17)$$

The vapour–liquid equilibrium at the interface is calculated with the Wilson equation, which is applicable for binary mixtures with no miscibility gap.

The thermophysical properties, particularly the multicomponent diffusion coefficients, depend on temperature and composition. They are calculated from pure component data by means of mixing rules which are applicable to ideal gas multicomponent mixtures. For further details on thermophysical data used here see ref. [15].

Information about inlet temperature, composition, pressure and velocity is still needed.

3. NUMERICAL METHOD

For the solution of the differential equations a computer code developed by Odenthal [13] has been extended to multicomponent mixtures. The numerical method is based on the finite difference method developed by Patankar and Spalding [18] and is outlined here briefly.

A transformed set of partial differential equations for the vapour–gas flow, equations (1)–(4) and (7)–(8), will be solved where the radial coordinate r is replaced by a dimensionless stream function ω. The resulting set of equations has the general form

$$\frac{\partial \phi}{\partial z} + a_\phi (1-\omega)\frac{\partial \phi}{\partial \omega} = \frac{\partial}{\partial \omega}\left(c_\phi d_\phi \frac{\partial \phi}{\partial \omega}\right) + e_\phi + f_\phi \frac{\mathrm{d}p}{\mathrm{d}z} \quad (18)$$

where ϕ denotes the dependent variables u, $\hat{h}$, ξ_i, k and ε.

The equations for u, k and ε are discretized, integrated over a finite volume and put into a tridiagonal matrix form at every coordinate z_i

$$\phi_i = \mathrm{A}_i \phi_{i+1} + B_i \phi_{i-1} + C_i + D_i \frac{\mathrm{d}p}{\mathrm{d}z}. \quad (19)$$

to solve numerically for the variables ϕ_i at the positions ω_i. Using inlet and boundary conditions and an estimate for the pressure gradient this system of equations can be solved. The iteration within the system can normally be omitted if small integration steps are chosen. However, the non-linear temperature dependence of the vapour–liquid equilibrium causes a strong coupling of the partial differential equations for $\hat{h}$ and ξ_i in the vapour–gas phase, the energy equation in the liquid and the corresponding balances at the interface. In addition the partial differential equations of $\hat{h}$ and ξ_i are coupled among each other by the source terms e_ϕ of equations (18) which includes the portions of diffusion in the heat flux and in the cross terms of the mass fluxes.

These effects lead to instabilities in the original uncoupled solution scheme. An iterative scheme where the tridiagonal matrices of each variable have been solved in turn did not lead to a convergent solution, either. Hence, a new scheme has been employed where the equations are solved simultaneously. Considering the complete dependencies in these equations and adding the energy equation in the liquid film and the concerning balances results in a band matrix with ten instead of three diagonals. This band matrix consists partly of non-linear coefficients so that a Newton algorithm for non-linear matrices has been applied to solve for the variables. With this solution scheme it is possible to calculate the coupled heat and mass transfer for any combination of values for inlet and boundary conditions. For further information on the derivatives and other details used in the solution scheme see ref. [15].

4. RESULTS AND DISCUSSION

The presented numerical approach is used to investigate multicomponent diffusion interactions in laminar and turbulent pipe flow. Since these diffusion interactions are not dominant for all inlet conditions and also depend on the diffusion and transport properties of the vapour–gas mixture there exist only a few experiments to directly examine multicomponent diffusion interactions. Therefore the available experiments are used only to validate the numerical approach. The effect of multicomponent diffusion interactions will be investigated instead by numerical experiments.

4.1. *Comparison with experiments*

Table 1 gives a survey of literature on condensation experiments with ternary mixtures in pipe flow. The experiments are distinguished by the existence of a miscibility gap in the liquid phase. For validation only the experiments with vapour components without a miscibility gap are used. Most experiments have been performed at normal pressure and in a Reynolds number range of 6000 to 30 000. Two authors published local measurements while the others give integral quantities for heat and mass transfer.

For the validations of the numerical approach some exemplary integral and local measurements have been chosen. For a detailed discussion of all experiments mentioned in Table 1, see ref. [15].

Modine [21] measured integral heat and mass transfer rates between a binary liquid film flowing down a wetted wall column and concurrently flowing vapour–gas mixture consisting of acetone, benzene and nitrogen or helium as the inert, to investigate multicomponent diffusion interactions. The column was operated adiabatically, so that the low boiling acetone is evaporating while the high boiling benzene is condensing. The own calculated and the measured changes between entrance and outlet of the film mass flow rate of both vapour components are shown in Fig. 2 and the corresponding temperature differences

Table 1. Experiments with ternary two-phase pipe flow

Mixture system			Inlet Reynolds number	p [bar]	Reference
In liquid phase miscible vapour components					
Acetone	methanol	air	20 000–40 000	1.013	von Behren *et al.* [19]
Acetone	benzene	nitrogen	940–4500	n.a	Toor and Sebulsky [20]
Acetone	benzene	nitrogen	10 500–20 500	1.19–1.55	Modine [21]
Acetone	benzene	helium	940–4500	n.a.	Toor and Sebulsky [20]
Acetone	benzene	helium	2000–9600	1.19–1.55	Modine [21]
Methanol	benzene	air	18 900–22 200	1.013	Mizushina *et al.* [22]
Methanol	water	air	11 800–23 300	1.013	Mizushina *et al.* [22]
n-Hexane	benzene	nitrogen	11 000–28 000	1.02	Lehr [23]
Benzene	toluene	nitrogen	6800–18 900	1.02	Lehr [23]
Isopropanol	water	nitrogen	6800–10 200	1	Webb and Sardesai [24]
Isopropanol	water	R12	10 500–19 800	1	Webb and Sardesai [24]
Isopropanol	*n*-butanol	nitrogen	43 000–220 000	4.95–10.96	Rennhack *et al.* [25], Lange [26]
In liquid phase immiscible vapour components					
Benzene	water	air	22 800	1.013	Mizushina *et al.* [22]
n-Heptane	water	R12	15 400–22 600	1	Sardesai [27]
Water	toluene	air	18 100	1.013	Mizushina *et al.* [22]
Water	toluene	R12	15 000–25 000	1	Sardesai [27]
Water	toluene	nitrogen	12 500–19 300	1	Sardesai [27]
Water	toluene	nitrogen	6500–9400	1	Deo [28]

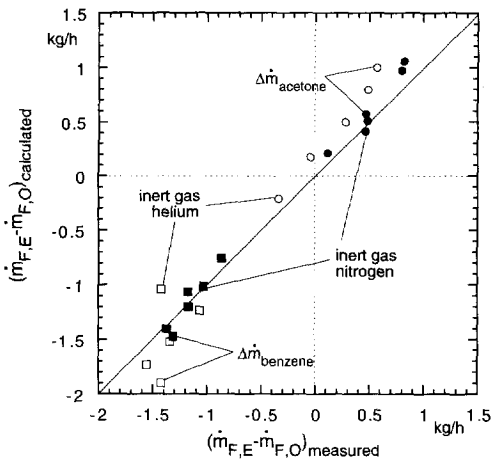

Fig. 2. Predicted and measured film mass flow rate difference; data from Modine [21].

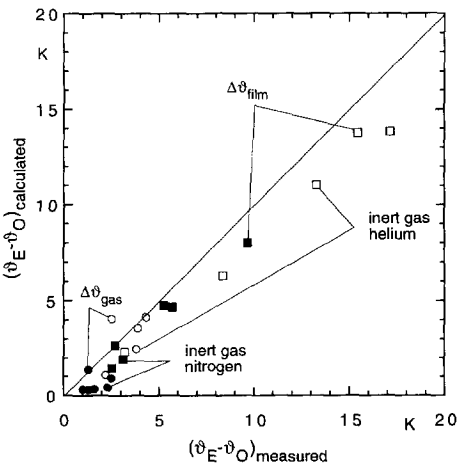

Fig. 3. Predicted and measured temperature differences; data from Modine [21].

between entrance and outlet of the gas flow and the liquid film are given in Fig. 3.

The differences of the mass transfer rates between measurements and calculation are about 5–77% for the mixture with nitrogen and 10–310% for that with helium. The large relative error of 310% was found for a run where the mass transfer rate of acetone is nearly zero. These errors seem to be rather large, but relative to the mass flow rate of the liquid film, which is always about 20 kg h^{-1} the differences between measurement and calculation are within the usual range of measurement errors.

The direction of the mass transport is always predicted correctly except the run where the mass transfer rate of acetone is nearly zero. This has also been noticed by Krishna [29] who compared results of his matrix method with Modine's measurements. The prediction of the temperature differences shows deviations of about 2 K for the system with nitrogen and about 3 K for the mixture with helium.

The comparison of calculated and measured condensation rates for the experiments of Webb and Sardesai [24] are shown in Fig. 4. The predicted values for isopropanol are good while those for water are 15–25% too low. There are probably two reasons for this underprediciton. Firstly, the inlet of the condenser consists of a T-junction. Sardesai noticed in his Ph.D. thesis an increase in pure heat transfer of 10–20% compared with a hydrodynamically developed flow but he did not investigate the effect of the T-junction on condensing flows [27]. The influence of the T-junction cannot be predicted by the numerical approach presented here due to its three-dimensionality. Second, applying the stability criteria of Ford and

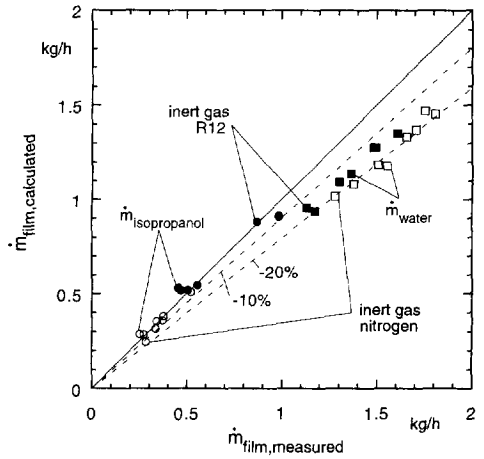

Fig. 4. Predicted and measured film mass flow rate; data from Webb and Sardesai [24].

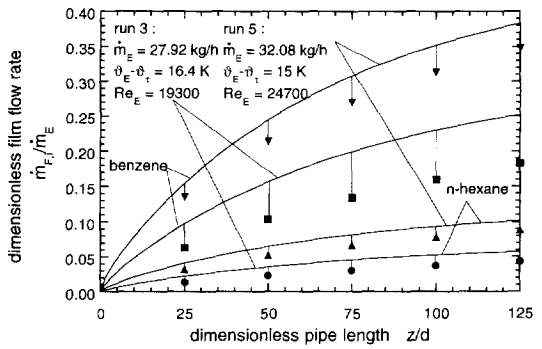

Fig. 5. Predicted and measured local film mass flow rates of component i; runs 3 and 5 by Lehr [23] with n-hexane–benzene–nitrogen.

Missen [30] for the stability of liquid binary films shows that these components tend to form an unstable streaky film. This effect leads to lower temperatures at the interface of the condensate film and to higher heat and mass transfer rates in the experiment. The temperature differences of the vapour–gas flow which are not presented here also are underpredicted and support these assumptions.

Predicted and measured local dimensionless film mass flow rates are shown in Fig. 5 for two runs of Lehr [23] for the system n-hexane–benzene–nitrogen and in Fig. 6 for a run of Rennhack *et al.* [25] and a run of Lange [26] for the system isopropanol–n-butanol–nitrogen. The mass transfer rates predicted for the experiments by Lehr are too large while those calculated for the experiments by Lange show fairly good agreement. The overprediction exists for all data of Lehr and confirms the results of McNaught [31] who found deviations in the same range for the models he considered. Due to this fact and the good results of Lange's experiments it is assumed that the causes for these differences should not be searched for in the numerical approach.

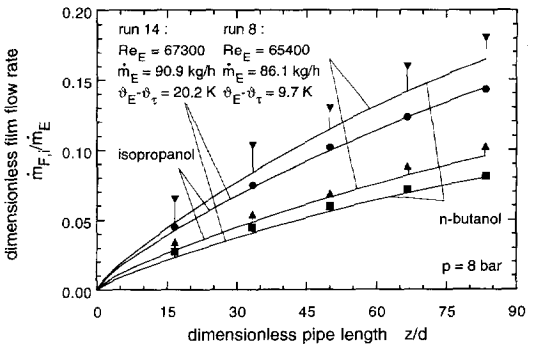

Fig. 6. Predicted and measured local film mass flow rates of component i; run 8 by Rennhack *et al.* [25] and 14 by Lange [26].

4.2. *Numerical experiments*

The comparison of the numerically predicted heat and mass transfer rates with experiments of several studies showed good results in a great range of gas Reynolds number. The measurements of Modine and Lange are predicted especially well and validate the presented computer code in the range of laminar flowing liquid film. It will now be used to perform some numerical experiments to investigate the influence of multicomponent diffusion interactions on laminar and turbulent condensing flow.

Firstly the 1D isothermal diffusion layer is considered to illustrate the diffusion interactions in a ternary mixture. For this system Toor investigated the conditions under which the phenomena diffusion barrier (the rate of diffusion of a component is zero even though its concentration gradient is not zero), osmotic diffusion (the rate of diffusion of a component is not zero even though its concentration gradient is zero) and reverse diffusion (a component diffuses countercurrent to the gradient of its concentration) occur [1].

Here the phenomena of osmotic diffusion are used to show how the concentration profiles depend on the differences of the binary diffusion coefficients in the mixture and the driving concentration difference of the other component. In Fig. 7 the mole fraction profiles in a 1D isothermal diffusion layer of the com-

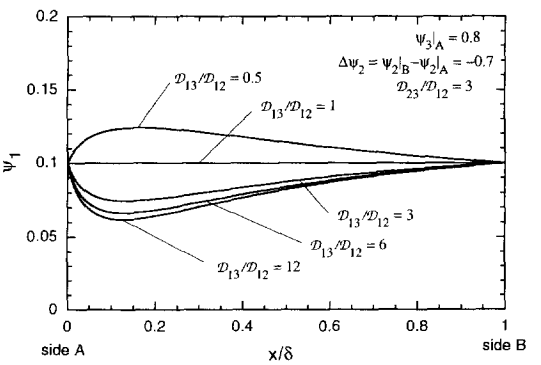

Fig. 7. Influence of the ratio of binary diffusion coefficients on mole fraction profiles in 1 D diffusion layer at osmotic diffusion.

ponent subject to osmotic diffusion are shown. The mole fraction and the molar reference frame for diffusion are chosen for Fig. 7 because in the mass reference frame an additional dependence on the components molecular masses appears. As the molecular masses also influence the diffusion coefficients, they cannot be chosen independently. The concentration of the first component is kept at the same value on both sides of the diffusion layer. At a large driving concentration difference of the second component $\Psi_{2|B} - \Psi_{2|A} = -0.7$ the ratio of the binary diffusion coefficients $\mathscr{D}_{13}/\mathscr{D}_{12}$ has been varied from 0.5 to 12. For ratios $\mathscr{D}_{13}/\mathscr{D}_{12} > 1$ the coupling with the second component leads to a decrease of the mole fraction up to a local minimum. On side B both gradients are cocurrent and result in a diffusion flux of the first component from side B to A. On side A the gradient of the first component is countercurrent to that of the second component and causes a negative diagonal term of the diffusion flux which is compensated by the positive cross term due to the coupling with the second component. With increasing ratio of $\mathscr{D}_{13}/\mathscr{D}_{12}$ and stronger coupling the local minimum and by this way the countercurrent gradient at side A increases. The coupling can be such that at ratios of $\mathscr{D}_{13}/\mathscr{D}_{12} < 1$ local maxima can be formed.

As a next example the condensation of isopropanol and *n*-butanol from a mixture with helium is considered to demonstrate the influence of multicomponent diffusion interactions in condensing flows. Since osmotic diffusion occurs only for the low boiling component in condensing flows it is enough to discuss the profiles of isopropanol.

In Fig. 8 the radial mass fraction profiles of isopropanol in laminar flow are compared with the corresponding profiles of a 1D diffusion layer. The thickness of the boundary layer has been applied to the simple diffusion layer. No liquid film was taken into account to omit changes of the interface temperature along the condenser wall. The wall temperature has been set so that the mass fraction of isopropanol at the interface is the same as at the inlet and osmotic diffusion occurs for this component.

The coupling of the concentration profiles generates local minima near the interface. With progressing condensation the cross sectional area increases where the mass fraction is lower as that on the axis. At a dimensionless pipe length of $z/d = 20$, the diffusion boundary layer reaches the axis. The location and the magnitude of the local minimum changes to larger wall distances. The 1D concentration profiles show similar local minima. The different locations of the minima are caused by the change of area perpendicular to the diffusion direction due to the pipe geometry. The multicomponent coupling in the condensing flow seems to be stronger due to the temperature dependence of the diffusion coefficients and the fluid density. Similar to the situation in laminar flows there are also local minima in the mass fraction profiles of the boiling component at osmotic diffusion in turbulent

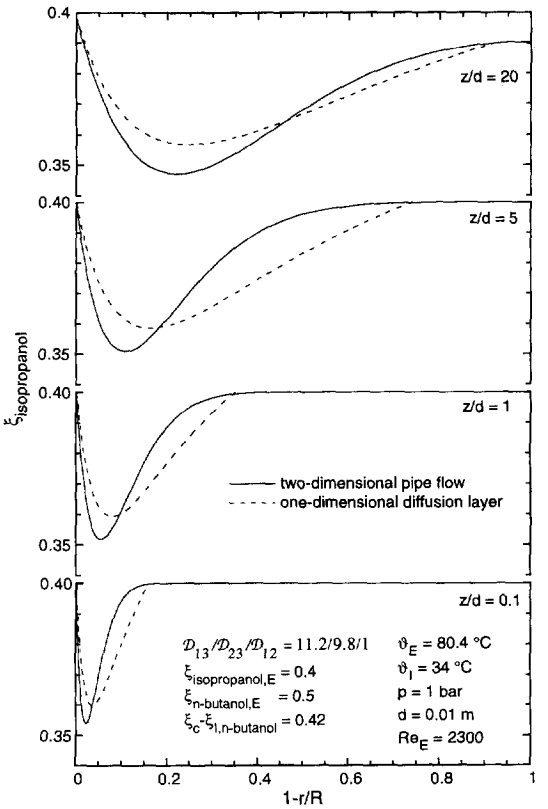

Fig. 8. Development of isopropanol mass fraction profiles in laminar condensation of isopropanol (1), *n*-butanol (2), helium (3) at osmotic diffusion.

flow, see Fig. 9. Location and magnitude of the minima depend on the Reynolds number. The coupling of concentration gradients seems to be limited to the near wall region with low turbulence. At a higher Reynolds number of $Re_E = 30\,000$ the local minima lie closer to the wall.

To get a more general insight into the influence of the turbulence on the multicomponent coupling the mass fraction profiles are made dimensionless similar to the well known dimensionless velocity u^+. The diagonal diffusion flux is used to make the profiles dimensionless. This has the advantage of gaining positive values even at reverse and osmotic diffusion.

$$\xi_1^+ = \frac{\rho u_\tau (\xi_1 - \xi_{1,l})}{\left(\rho D_{11} \dfrac{\partial \xi_1}{\partial y}\right)_l} \qquad \xi_2^+ = \frac{\rho u_\tau (\xi_2 - \xi_{2,l})}{\left(\rho D_{22} \dfrac{\partial \xi_2}{\partial y}\right)_l}$$

$$\text{and} \quad y^+ = \frac{y u_\tau}{\nu} \tag{20}$$

with

$$u_\tau = \sqrt{\frac{\left(\eta \dfrac{\partial u}{\partial y}\right)_l}{\rho_l}}. \tag{21}$$

In Fig. 10 these profiles are shown for several inlet

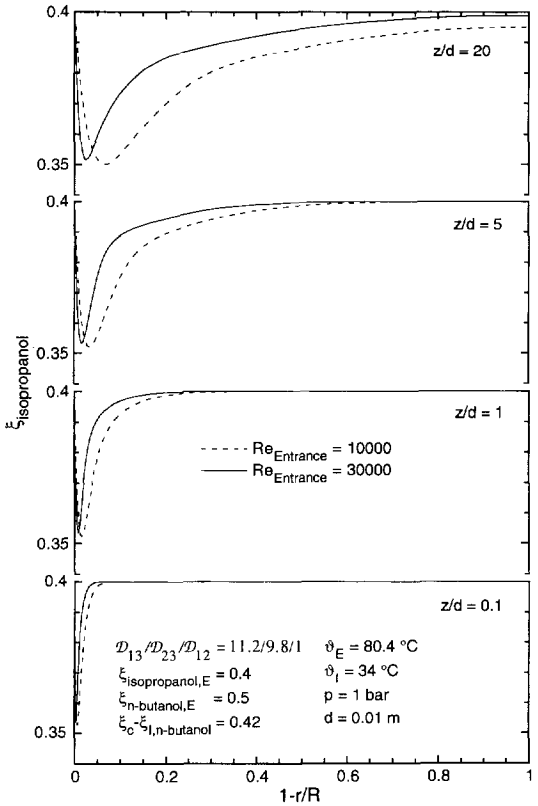

Fig. 9. Development of isopropanol mass fraction profiles in turbulent condensation of isopropanol (1), *n*-butanol (2), helium (3) at osmotic diffusion.

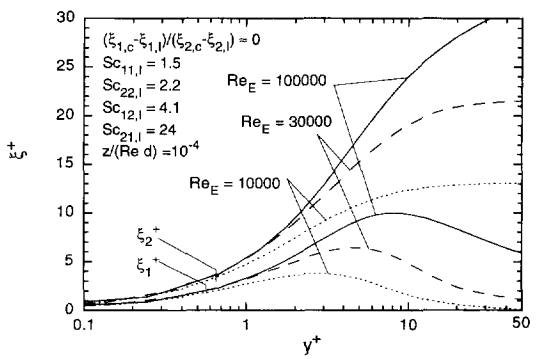

Fig. 10. Influence of Reynolds number on coupling of mass fraction profiles in turbulent condensation of isopropanol (1), *n*-butanol (2), helium (3) at osmotic diffusion.

Reynolds numbers as a function of the dimensionless wall distance y^+. The profiles are taken at a local dimensionless coordinate of $z/(Re\ d) = 10^{-4}$ to take into account the effects of the hydrodynamic development of the boundary layer at different Reynolds numbers. In this graph the minima of the mass fraction profiles convert to local maxima. At the low Reynolds number the maximum lies in the viscous sublayer ($y^+ < 5$). With growing Reynolds number the maximum moves to higher values of y^+ into the buffer layer. This means that the coupling of the concentration gradients increases with higher turbulence.

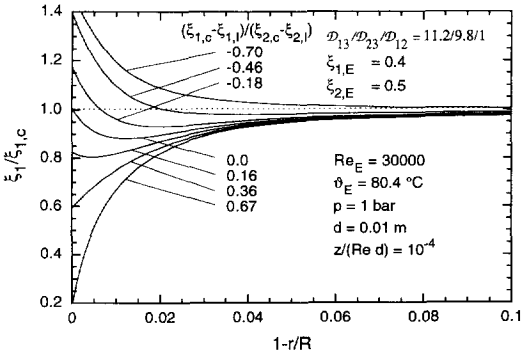

Fig. 11. Influence of driving concentration difference of *n*-butanol on isopropanol mass fraction profiles in turbulent condensation of isopropanol (1), *n*-butanol (2), helium (3).

This seems to be in contrast to equation (7) where it can be seen that turbulent diffusion increases the diagonal term and lowers the effect of cross terms. But this can be explained by looking at the ξ_2^+-profiles in Fig. 10. With growing Reynolds number the gradient of the second component increases at the border of the buffer layer and due to the direct coupling of the concentration profiles the cross diffusion partially compensates the turbulent diffusion.

The influence of the driving concentration difference of the second component on the mass fraction profile of the first component can be seen in Fig. 11. The mass fractions have been divided by the value at the pipe axis. The inlet conditions have been kept constant. The various driving concentration differences are generated by changing the wall temperature. For a concentration ratio of $(\xi_{1,c}-\xi_{1,I})/(\xi_{2,c}-\xi_{2,I}) = -0.7$ a typical profile of reverse diffusion exists. The mass fraction at the liquid interface is high and decreases continuously with increasing wall distance. If the concentration difference of the first component becomes lower (ratio equal to -0.46) a local minimum arises which has its most distinct form at the point of osmotic diffusion and is still existent if the direction of the driving concentration difference of both components is the same. That means that reverse diffusion still exists even at cocurrent driving forces for the mass transfer. Obviously the concentration gradients at the gas/liquid interface cannot be predicted considering only the driving concentration differences, as is done in one-dimensional approaches using linearized theories or matrix methods, and a complete solution of the partial differential equations is required.

These results confirm those of Sage and Estrin [6] who examined condensation of steam from a ternary mixture with two non-condensables in a laminar boundary layer. In the system nitrogen–Freon–water they observed a local minimum in the concentration profile and a buildup of the non-condensable Freon at the interface of the condensate film. These effects have also been shown in the system nitrogen–neon–water, but are not so strong due to the weaker coupling in this system.

5. CONCLUSIONS

An approach based on a numerical solution of the 2D conservation equations has been proposed to calculate heat and mass transfer of ternary mixtures in laminar and turbulent pipe flow and validated by comparison with local and integral experimental results of several studies over a wide range of Reynolds numbers. The validated approach has been used to perform some numerical experiments to investigate the influence of multicomponent diffusion interactions at the point of osmotic diffusion.

Local minima in the concentration profiles occur for the component subject to osmotic diffusion. A comparison with the profiles in 1D diffusion layer shows that the temperature dependence of density and binary diffusion coefficients strengthens the coupling of the concentration profiles in laminar flow.

In turbulent flow the local minima move with increasing Reynolds number from the viscous sublayer into the buffer layer. As a result of a larger concentration gradient of the second component at higher turbulence, the cross diffusion term partially compensates the turbulent diffusion of the first component.

The variation of the driving concentration differences shows local minima of the mass fraction profiles in a large range of concentration differences. Multicomponent diffusion interactions lead to reverse concentration gradients even at cocurrent driving concentration differences.

Acknowledgement—The authors wish to acknowledge the Deutsche Forschungsgemeinschaft (German Science Foundation) for financial support.

REFERENCES

1. H. L. Toor, Diffusion in three-component gas mixtures, *A.I.Ch.E. Jl* **3**(2), 198–207 (1957).
2. H. L. Toor, Solution of the linearized equations of multicomponent mass transfer—I, *A.I.Ch.E. Jl* **10**(4), 448–460 (1964).
3. W. E. Stewart and R. Prober, Matrix calculation of multicomponent mass transfer in isothermal systems, *I & EC Fundam.* **3**(3), 224–235 (1964).
4. R. Krishna and G. L. Standart, Mass and energy transfer in multicomponent systems, *Chem. Engng Commun.* **3**, 201–275 (1979).
5. Y. Taitel and A. Tamir, Film condensation of multicomponent mixtures, *Int. J. Multiphase Flow* **1**, 697–714 (1974).
6. F. E. Sage and J. Estrin, Film condensation from a ternary mixture of vapors upon a vertical surface, *Int. J. Heat Mass Transfer* **19**, 323–333 (1976).
7. H. Kosuge, T. Ishikawa and K. Asano, Numerical analysis of ternary mass transfer in a laminar boundary layer, *J. Chem. Engng Japan* **20**(5), 525–530 (1987).
8. S. Bröcker, Allgemeine Näherungslösung für den Stoffaustausch in laminaren Mehrstoffgrenzschichten an der längs angeströmten, ebenen Platte, Ph.D. Thesis, TU Braunschweig (1991).
9. S. Bröcker, Eine neue, allgemeine Näherungslösung für den Wärme- und Stoffaustausch in laminaren Mehrstoffgrenzschichten an der längs angeströmten, ebenen Platte, *Wärme-und Stoffübertragung* **28**(6), 329–340 (1993).
10. R. Taylor, On multicomponent mass transfer in turbulent flow, *Lett. Heat Mass Transfer*, **8**, 397–404 (1981).
11. R. Krishna, Multicomponent mass transfer in turbulent flow, *Lett. Heat Mass Transfer* **8**, 195–206 (1981).
12. U. Renz, Die partielle Filmkondensation aus laminaren und turbulenten Grenzchichtströmungen, *Lett. Heat Mass Transfer* **2**, 9–12 (1975).
13. H. P. Odenthal, Berechnung des Wärme- und Stoffaustauschs bei partieller Kondensation in turbulent durchströmten Kondensatorrohren, Ph.D. Thesis, RWTH Aachen (1983).
14. W. W. Baumann and F. Thiele, Heat and mass transfer in evaporating two-component liquid film flow, *Int. J. Heat Mass Transfer* **33**(2), 267–273 (1990).
15. M. Braun, Wärme- und Stoffaustausch bei der Kondensation von ternären Gas-/Dampfgemischströmungen, Ph.D. Thesis, RWTH Aachen (1995).
16. W. P. Jones, B. E. Launder, The prediction of laminarization with two-equation model of turbulence, *Int. J. Heat Mass Transfer* **15**, 301–314 (1972).
17. H. Kawamura, Analysis on laminarization of heated gas using a two equation model of turbulence, *Proceedings of 2nd Symposium on Turbulent Shear Flow*, pp. 1816–1821. Imperial College London (1979).
18. S.V. Patankar and D. B. Spalding, *Heat and Mass Transfer in Boundary Layers*. Intertext Books, London (1970).
19. G. L. von Behren, W. O. Jones and D. T. Wasan, Multicomponent mass transfer in turbulent flow, *A.I.Ch.E. Jl* **18**(1), 25–30 (1972).
20. H. L. Toor and R. T. Sebulsky, Multicomponent mass transfer—II. Experiment, *A.I.Ch.E. Jl.* **7**(4), 565–573 (1961).
21. A. D. Modine, Ternary mass transfer, Ph.D. Thesis, Carnegie-Mellon University of Pittsburgh (1963).
22. T. Mizushine, H. Ueda, S. Ikeno and K. Ishii, Simplified calculation for cooler condensers for gas-multicomponent vapour mixtures, *Int. J. Heat Mass Transfer* **7**, 95–100 (1964).
23. G. Lehr, Wärme- und Stoffübergang bei der Kondensation von zwei Dämpfen aus einem Gemisch mit einem Inertgas, Ph.D. Thesis, TU Hannover (1972).
24. D. R. Webb and R. G. Sardesai, Verification of multicomponent mass transfer models for condensation inside a vertical tube, *Int. J. Multiphase Flow* **7**(5), 507–520 (1981).
25. R. Rennhack, R. Numrich and J. Lange, Die Kondensation zweier im flüssigen Zustand löslicher Komponenten aus einem Gas/Dampfgemisch bei erhöhtem Druck, Abschlußbericht des AiF-Forschungsvorhabens Nr. 7888 Köln, Arbeitsgemeinschaft industrieller Forschungsvereinigungen (1993).
26. J. Lange, Die partielle Kondensation zweier im flüssigen Zustand löslicher Komponenten aus einem Gas-Dampfgemisch im senkrechten Rohr bei erhöhtem Druck, Ph.D. Thesis, University-GH Paderborn (1995).
27. R. G. Sardesai, Studies in condensation, Ph.D. Thesis, UMIST, University of Manchester (1979).
28. P. V. Deo, Condensation of mixed vapours, Ph.D. Thesis, UMIST, University of Manchester (1979).
29. R. Krishna, Ternary mass transfer in a wetted-wall column, significance of diffusional interactions—I. Stefan diffusion, *Trans. IChemE* **59**, 35–43 (1981).
30. J. D. Ford and R. W. Missen, On the conditions for stability of falling films subject to surface tension disturbances; the condensation of binary vapors, *Can. J. Chem. Engng.* **46**, 309–312 (1968).
31. J. M. McNaught, An assessment of design methods for condensation of vapors from a noncondensing gas. In *Heat Exchangers, Theory and Practice* (Edited by J. Taborek, G. F. Hewitt and N. Afgan), pp. 35–53. Hemisphere, Washington, DC (1983).